Universiteit
Leiden
The Netherlands

Structural and functional models for [NiFe] hydrogenase

Angamuthu, R.

Citation
Angamuthu, R. (2009, October 14). *Structural and functional models for [NiFe] hydrogenase*. Retrieved from https://hdl.handle.net/1887/14052

Version:	Corrected Publisher's Version
License:	Licence agreement concerning inclusion of doctoral thesis in the Institutional Repository of the University of Leiden
Downloaded from:	https://hdl.handle.net/1887/14052

Note: To cite this publication please use the final published version (if applicable).

5

Heterodinuclear [NiRu] Complexes Comprising Ruthenium Bis-Bipyridine: Synthesis, Characterisation and Electrocatalytic Dihydrogen Production†

Abstract. Three new heterodinuclear $[Ni(S_2S'_2)Ru(bpy)_2](PF_6)_2$ complexes have been synthesized by the reaction between $[Ni(S_2S'_2)]$, *in situ* formed *cis*-$[Ru(bpy)_2(EtOH)_2]Cl_2$, and NH_4PF_6 in which $[Ni(S_2S'_2)]$ is [Ni(pbss)], [Ni(pbsms)] and [Ni(xbsms)]. The three $[Ni(S_2S'_2)Ru(bpy)_2](PF_6)_2$ complexes have been characterized by ESI-MS spectrometry, electronic absorption and NMR spectroscopy, electrochemical techniques and elemental analysis. The complex $[Ni(pbss)Ru(bpy)_2](PF_6)_2$ crystallizes in the space group $P2_1/c$; the heterodinuclear molecules are connected through a number of strong non-classical hydrogen bonds such as C–H···F, C–H···S and C–H···N, and as well as π···π interactions in the crystal lattice. All the three $[Ni(S_2S'_2)Ru(bpy)_2](PF_6)_2$ complexes have been found to reduce protons electrocatalytically in the presence of trifluoroacetic acid at potentials as low as –1.0 V *vs*. Ag/AgCl in acetonitrile. The complexes have been found to be tolerant towards higher concentrations of acid.

---

† R. Angamuthu, M. A. Siegler, A. L. Spek and E. Bouwman, *manuscript in preparation*.

5.1. Introduction

Heterodinuclear [NiRu][1-6] and homodinuclear [RuRu][7,8] complexes reported in recent literature exhibit exciting properties, such as suitable structural and functional mimics of nickel-containing enzymes, especially hydrogenases. Even though high-resolution X-ray crystal structures are available for the [NiFe] hydrogenases isolated from *D. gigas*,[9,10] *D. vulgaris*,[11-14] *D. fructosovorans*,[15-17] *D. sulfuricans*[18] and *Dm. baculatum*[19] and studying [NiFe] complexes as models would be meaningful, the following reasons can be considered to use Ru(II) instead of Fe(II) in the model complexes: **(1)** Ru(II) shows high affinity towards H_2,[20] **(2)** Ru(II) complexes are comparatively much more stable with respect to the corresponding Fe(II) counterparts, and **(3)** Ru(II) complexes of amine ligands are well known for their photoactivity in combination with their redox activity while the Fe(II) counterparts are only redox-active.

The photocatalytic splitting of water into dihydrogen and dioxygen, and the light-driven proton reduction into molecular hydrogen are both known to have been catalyzed by combining a light-absorbing photoactive center with a redox-active center. Three common approaches reported in the literature to develop light-assisted redox reactions are: **(1)** a photo-active center, e.g. $[Ru(bpy)_3]^{2+}$, is connected to the redox-active center by a conjugated system (see Fig. 1.17A);[21-24] **(2)** the photo-active center is separated from the redox-active center by a non-covalently binding linker (see Fig. 1.17B);[25-27] **(3)** the photo-active center is active in combination with sacrificial electron donors.[25,28-30]

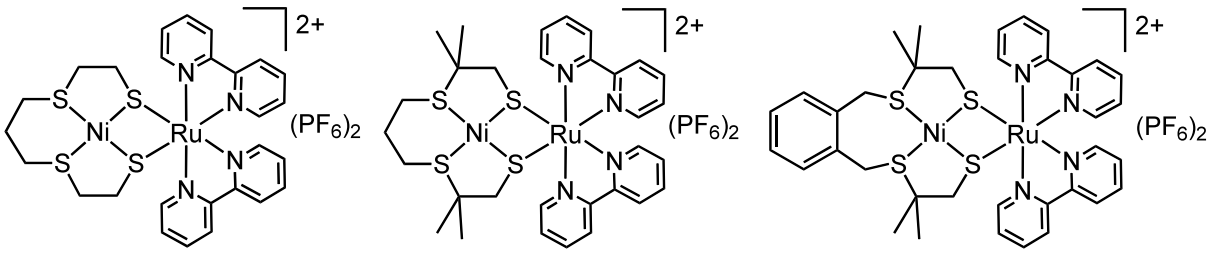

$[Ni(pbss)Ru(bpy)_2](PF_6)_2$ $[Ni(pbsms)Ru(bpy)_2](PF_6)_2$ $[Ni(xbsms)Ru(bpy)_2](PF_6)_2$

Fig. 5.1 Schematic structures of the heterodinuclear [NiRu] complexes described in this Chapter.

This Chapter is devoted to the study of a new approach by designing heterodinuclear [NiRu] complexes containing a redox-active NiS_4 unit directly connected to a photoactive group such as $[Ru(bpy)_2]^{2+}$, as shown in Fig. 5.1. The synthesis, structure and electrocatalytic properties of the three [NiRu] complexes $[Ni(pbss)Ru(bpy)_2](PF_6)_2$,

[Ni(pbsms)Ru(bpy)$_2$](PF$_6$)$_2$ and [Ni(xbsms)Ru(bpy)$_2$](PF$_6$)$_2$, synthesized using the mononuclear nickel complexes [Ni(pbss)], [Ni(pbsms)] and [Ni(xbsms)], respectively, are reported in this Chapter (Fig. 5.1).

5.2. Results

5.2.1. Synthesis

The syntheses and characterizations of the $S_2S'_2$-donor ligands and of their mononuclear low-spin nickel(II) complexes have been discussed in Chapters **2** and **3**, respectively. The complex [Ru(bpy)$_2$(EtOH)$_2$]Cl$_2$ is formed *in situ* and reacted with mononuclear nickel(II) complexes [Ni(pbss)], [Ni(pbsms)] and [Ni(xbsms)] in 1:1 ratio in ethanol to obtain the complexes [Ni(pbss)Ru(bpy)$_2$]Cl$_2$, [Ni(pbsms)Ru(bpy)$_2$]Cl$_2$ and [Ni(xbsms)Ru(bpy)$_2$]Cl$_2$, respectively (Scheme 5.1). The chloride anions are exchanged with PF_6^- anions using an excess (amount) of NH_4PF_6. The [NiRu] complexes have been isolated in analytically pure crystalline form and were used without further purifications. The presence of the PF_6^- anions is visible in the IR spectra of the complexes with strong bands around 830 cm^{-1}.

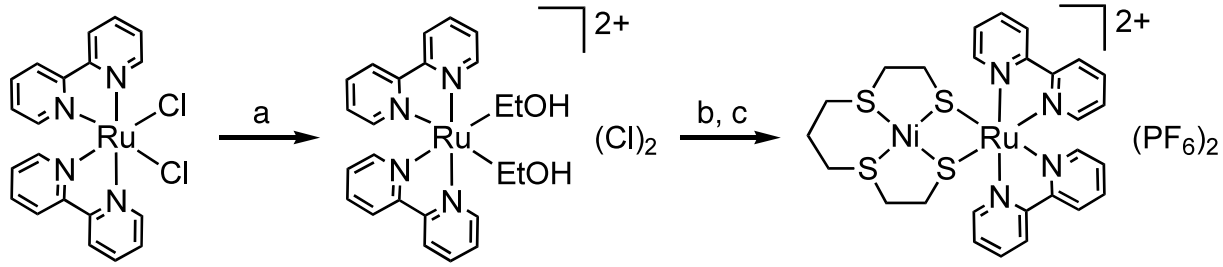

Scheme 5.1. Illustrative synthetic route used in the synthesis of [NiRu] complexes; (a) ethanol, reflux, 2 hrs; (b) [Ni(pbss)], reflux, 6 hrs; (c) NH_4PF_6, stirring, 15 minutes.

5.2.2. Molecular Structure of the [NiRu] Complexes

Perspective views of the molecular structure of the cation [Ni(pbss)Ru(bpy)$_2$]$^{2+}$ are shown in Fig. 5.2; selected interatomic distances and angles are provided in Table 5.1 along with the data of [Ni(pbss)][31] for comparison. The asymmetric unit of [Ni(pbss)Ru(bpy)$_2$](PF$_6$)$_2$ contains one crystallographically independent, ordered molecule. The [Ni(pbss)] unit in [Ni(pbss)Ru(bpy)$_2$]$^{2+}$ retains the square-planar geometry around the Ni(II) ion with two thiolate donors and two thioether sulfurs in enforced *cis* positions. The two thiolate donors of [Ni(pbss)] are connected to the *cis*-[Ru(bpy)$_2$]$^{2+}$ unit making a NiS_2Ru metallacycle through two Ni–S–Ru bridges; the [Ru(bpy)$_2$]$^{2+}$ group is situated at the same side of the Ni(II) coordination plane as the propylene-bridge of the pbss ligand, the four remaining sulfur lone pairs are all below the plane of coordination.

The Ni–$S_{thiolate}$ distances [2.1632(6), 2.1748(6) Å] are slightly shorter than the Ni–$S_{thioether}$ distances [2.1827(6)-2.1893(6) Å], as expected. However, this observation is in contrast to the parent complex [Ni(pbss)], where the Ni–$S_{thiolate}$ distances are slightly longer than the Ni–$S_{thioether}$ distances; usually, the Ni–$S_{thioether}$ distances are longer than (or similar to) the Ni–$S_{thiolate}$ distances (Table 5.1).[32,33] The fact that the two Ni–$S_{thiolate}$ bonds are slightly shorter in [Ni(pbss)Ru(bpy)$_2$](PF_6)$_2$ compared to the parent complex [Ni(pbss)], must be induced by the binding of thiolate sulfurs with ruthenium; the minimised repulsion between the π orbitals of nickel and the thiolate sulfurs upon binding to ruthenium allows for stronger Ni–$S_{thiolate}$ bonds. This observation is in line with the reported structure of [Ni(pbss)Fe(C_5H_5)(CO)](PF_6), in which the binding of the [Fe(C_5H_5)(CO)]$^+$ moiety also results in shortening of the Ni–$S_{thiolate}$ distances.[34]

Table 5.1. Selected distances (Å) and angles (°) for [Ni(pbss)Ru(bpy)$_2$](PF_6)$_2$. Distances and angles found in [Ni(pbss)] are provided in square brackets for comparison.[31]

Ni1–S6	2.1632(6) [2.179(2)]	Ni1–S9	2.1827(6) [2.173(1)]
Ni1–S16	2.1748(6) [2.177(2)]	Ni1–S19	2.1893(6) [2.166(2)]
Ru1–S6	2.4006(5)	Ru1–S16	2.3769(6)
Ru1–N1	2.0599(17)	Ru1–N2	2.0671(18)
Ru1–N3	2.066(2)	Ru1–N4	2.053(2)
S6–Ni1–S9	91.66(2) [90.17(6)]	S6–Ni1–S16	85.05(2) [87.05(6)]
S6–Ni1–S19	174.99(2) [175.85(6)]	S9–Ni1–S16	176.41(3) [177.02(6)]
S9–Ni1–S19	91.73(2) [92.85(5)]	S16–Ni1–S19	91.46(2) [89.87(5)]
Ru1–S6–Ni1	92.17(2)	Ru1–S16–Ni1	92.53(2)
S6–Ru1–S16	75.72(2)	S6–Ru1–N1	173.51(5)
S6–Ru1–N2	103.11(5)	S6–Ru1–N3	86.02(5)
S6–Ru1–N4	97.64(5)	S16–Ru1–N1	97.92(5)
S16–Ru1–N2	92.75(5)	S16–Ru1–N3	95.45(6)
S16–Ru1–N4	171.88(5)	N1–Ru1–N2	78.20(7)
N1–Ru1–N3	93.42(7)	N1–Ru1–N4	88.59(7)
N2–Ru1–N3	169.02(7)	N2–Ru1–N4	93.33(7)
N3–Ru1–N4	79.24(8)		

The nickel center has a slight tetrahedral distortion with a dihedral angle of 3.99°, as defined by the triangular planes S6Ni1S9 and S16Ni1S19. The S–Ni–S angles in [Ni(pbss)Ru(bpy)$_2$](PF_6)$_2$ have undergone a considerable degree of reorganization upon binding to the *cis*-[Ru(bpy)$_2$]$^{2+}$ moiety. Especially the S6–Ni1–S16 angle has decreased with almost 2.5° and the S9–Ni1–S19 angle enlarged nearly 3.5°, to accommodate the formation of the S6–Ru1–S16 hinge. The ruthenium center is in a distorted octahedral geometry with an N_4S_2 chromophore; the Ru–N [2.053(2)–2.0671(18) Å] and Ru–S [2.4006(5) and 2.3769(6) Å] distances are in the expected range and similar to related compounds.[35,36] The Ru–N bonds *trans* to the thiolate sulfur [Ru1–N1, 2.0599(17); Ru1–N4, 2.053(2) Å] are slightly shorter than the two other Ru–N bonds [Ru1–N2, 2.0671(18);

Ru1–N3, 2.066(2) Å]. The pyridyl ring A is tilted towards the methylene protons of the C1 and C3 carbons of the ligand pbss with H···H distances of 2.12 and 2.24 Å, respectively (Fig 5.2, right). The extended solid-state structure of [Ni(pbss)Ru(bpy)$_2$](PF$_6$)$_2$ is formed by a mixture of Δ and Λ enantiomers connected through a number of non-classical inter- and intra-molecular hydrogen-bonding networks of distances (H···A) ranging between 2.44 and 2.82 Å, and π···π stacking interactions of centroid-to-centroid distances ranging between 3.8202(15) and 5.8998(16) Å.

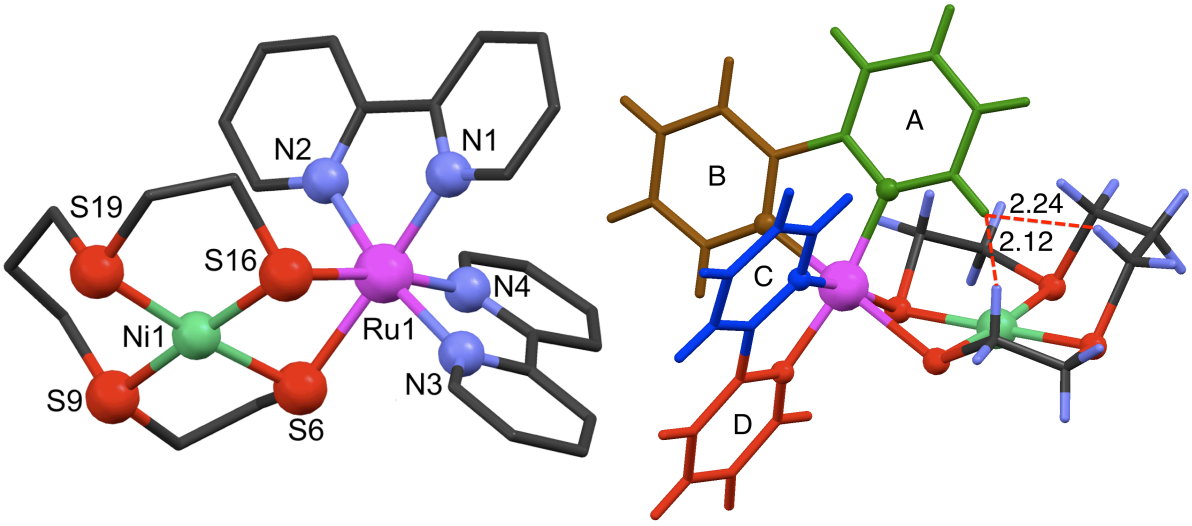

Fig. 5.2. Perspective views of the cationic part of [Ni(pbss)Ru(bpy)$_2$](PF$_6$)$_2$ showing the atomic numbering scheme; Ni1···Ru1, 3.2919(3) Å. Further details are provided in Table 5.1.

5.2.3. ESI-MS and Electronic Absorption Spectra of the [NiRu] Complexes

The ESI-MS spectrometric, and electronic absorption spectroscopic data of the [NiRu] complexes in acetonitrile and dichloromethane are provided in Table 5.2. All the three [NiRu] complexes exhibit the parent molecular-ion peak at *m/z* = [M-(PF$_6$)$_2$]$^{2+}$ in their corresponding ESI–MS spectra confirming the formulation [Ni($S_2S'_2$)Ru(bpy)$_2$]$^{2+}$.

In the electronic absorption spectra, all the [NiRu] complexes exhibit strong sharp absorption maxima around 34000 cm^{-1} corresponding to the intraligand (bpy) π–π* transition and a shoulder 28000 cm^{-1} corresponding to the LMCT of the NiS_4 chromophore. These complexes also show broad bands between 20000 and 22000 cm^{-1} with an extended shoulder (~18000 cm^{-1}) that are ascribed to Ru(4dπ)→π*(bpy) MLCT transition or a mixture of Ru(4dπ)→π*(bpy) MLCT transition and the characteristic d-d transition ($1E' \leftarrow {}^1A_1'$) of the NiS_4 chromophore. The removal of part of the electron density of the π-donating sulfur lone pairs by the coordination of the ruthenium center results in a slight blue-shift of the d-d transition of the nickel ion, as compared to the parent [Ni(pbss)] complex.

A recent report with a combination of experimental studies and DFT calculations of electronic absorption spectroscopic transitions from the group of Lever assigned the low intensity shoulders around 15000 cm^{-1} to Ru(4d)/S→π* bpy transitions;[37] the report concluded that an impressive number of actual electronic transitions are lying underneath the simple band envelope observed in the electronic absorption spectra of the ruthenium bis-bipyridine complexes. The interaction of coordinating solvents, such as acetonitrile, can be excluded, as the electronic spectra of the three [NiRu] complexes are quite similar in both acetonitrile and dichloromethane, and peaks for acetonitrile-solvated species are not observed in the ESI-MS spectra.

Table 5.2. Electronic absorption maxima for the $[Ni(S_2S'_2)Ru(bpy)_2](PF_6)_2$ complexes and the observed *m/z* values of the parent molecular-ion peaks.

Complex	$\nu/10^3$ cm^{-1} ($\varepsilon/10^3$ mol^{-1} l cm^{-1})		*m/z*
	Acetonitrile	Dichloromethane	exptl. (calcd.)
$[Ni(pbss)Ru(bpy)_2](PF_6)_2$	41.8(17.5) 34.5(32.6) 28.3(sh) 22.0(4.4) 17.9(sh) 14.9(sh)	40.3(sh) 34.6(39.2) 28.1(sh) 21.6(5.6) 18.0(sh) 14.9(sh)	348.80 (348.99)
$[Ni(pbsms)Ru(bpy)_2](PF_6)_2$	41.3(29.8) 34.6(50.8) 28.2(sh) 21.7(7) 17.9(sh) 15.1(sh)	40.2(sh) 34.5(49.4) 28.3(sh) 20.9(7.2) 18.0(sh) 14.9(sh)	376.86 (377.02)
$[Ni(xbsms)Ru(bpy)_2](PF_6)_2$	41.3(28.1) 34.6(50) 28.2(sh) 21.5(6.4) 18.0(sh) 15.0(sh)	39.8(sh) 34.4(4.5) 28.1(sh) 20.5(5.7) 18.0(sh) 15.0(sh)	407.72 (408.03)

5.2.4. NMR Spectroscopic Studies of the [NiRu] Complexes

The NMR spectra of the [NiRu] complexes were recorded using acetone-d6 solutions at different temperatures ranging between 223 and 303 K. The assignments of the protons and carbons are made unequivocally, based on the 1D ^1H and ^{13}C, and 2D homonuclear ^1H-^1H COSY, TOCSY, NOESY (T_{mix} = 1 s and 0.5 s), ROESY and heteronuclear ^1H–^{13}C HSQC spectra of the [NiRu] complexes. The assignments of the proton resonances are provided in Table 5.3. The numbering scheme of the protons and carbons of the three [NiRu] complexes is shown in Fig. 5.3.

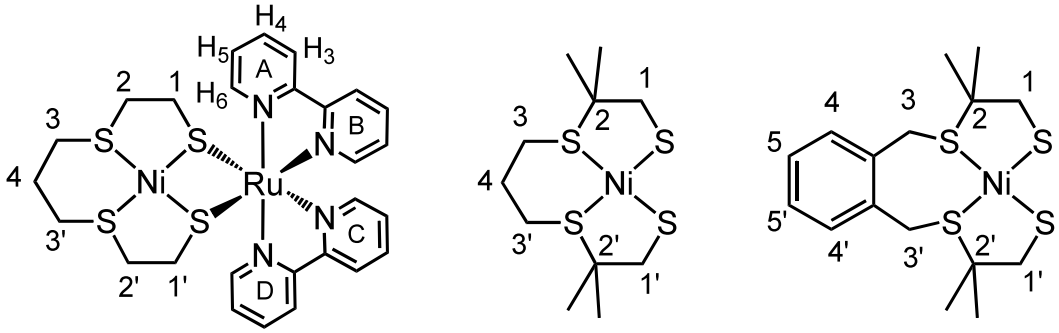

Fig. 5.3. Numbering scheme followed in the assignments of protons and carbons in the NMR spectra of the [NiRu] complexes.

The ^{1}H NMR spectra of the complexes [Ni(pbss)Ru(bpy)$_2$](PF$_6$)$_2$ and [Ni(xbsms)Ru(bpy)$_2$](PF$_6$)$_2$ show four sets of individual resonances for the four available pyridyl rings at all temperatures ranging from 233 to 303 K. The ^{1}H NMR spectrum of [Ni(xbsms)Ru(bpy)$_2$](PF$_6$)$_2$ in acetone-d6 is given in Fig. 5.4 as an example. The complex [Ni(pbsms)Ru(bpy)$_2$](PF$_6$)$_2$, however, shows four sets of broad resonances at 303 K, which resolve to eight sharp sets of resonances upon cooling the sample down to 233 K. The methylene protons of all the three complexes show sharp AB pattern signals (dd), due to the geminal coupling at low temperatures and broad signals/doublets at room temperature.

Table 5.3. ^{1}H NMR spectral data for the [Ni(S$_2$S'$_2$)Ru(bpy)$_2$](PF$_6$)$_2$ complexes recorded in acetone-d6 solutions.*

Complex	Chemical shift δ (ppm)					
	Pyridyl protons					Other protons
	Ring	H_3	H_4	H_5	H_6	
[Ni(pbss)Ru(bpy)$_2$](PF$_6$)$_2$	A	8.38	8.13	7.6	10.02	3.65 (3), 3.43 (3') 3.16–2.89 (2,2',4,4'), 2.1 & 1.84 (1), 1.3 & 0.8 (1')
	B	8.32	8.04	7.5	9.37	
	C	8.23	7.8	7.13	7.68	
	D	8.18	7.7	7.1	7.52	
[Ni(pbsms)Ru(bpy)$_2$](PF$_6$)$_2$	A	8.95	8.55	8.25	10.7	3.6–3.25 (3,3'), 2.9 (1), 2.8 (1), 2.53 (1), 2.55 (1), 1.94 (1'), 1.83 (1'), 1.2 (1'), 1.1 & 0.8 (1'), 1.9 (4), 1.66–1.19 (8Me),
		8.9		8.15	10.6	
	B	8.81	8.45	8.0	9.7	
		8.79			9.6	
	C	8.74	8.36	7.49	7.9	
		8.7		7.45		
	D	8.68	8.32	7.42	7.86	
		8.64		7.39	7.78	
[Ni(xbsms)Ru(bpy)$_2$](PF$_6$)$_2$	A	8.9	8.4	8.03	10.63	7.65 (4), 7.6 (4'), 7.54 (5), 7.5 (5'), 4.97 & 4.94 (3), 4.26 & 4.16 (3'), 2.51 & 1.85 (1), 1.82 (2Me, eq), 1.67 (2Me, ax), 1.64 (2'Me, eq), 1.61 (3'), 1.55 & 0.75 (1'), 1.46 (2'Me, ax),
	B	8.85	8.4	7.99	9.81	
	C	8.72	8.1	7.45	8.26	
	D	8.72	8.09	7.4	7.85	

* Presented data obtained for [Ni(pbss)Ru(bpy)$_2$](PF$_6$)$_2$ at 293 K, and for [Ni(pbsms)Ru(bpy)$_2$](PF$_6$)$_2$ and [Ni(xbsms)Ru(bpy)$_2$](PF$_6$)$_2$ at 233 K; see Fig. 5.3 for the numbering scheme.

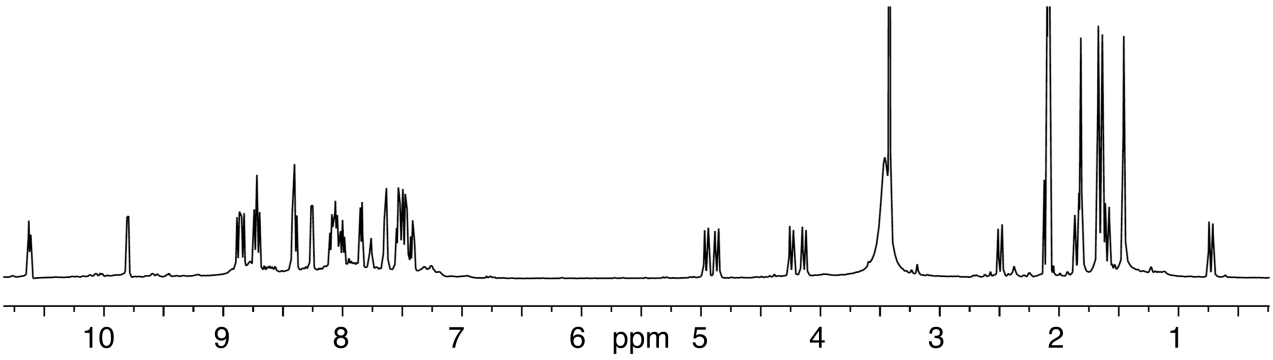

Fig. 5.4. ^{1}H NMR spectra of [Ni(xbsms)Ru(bpy)$_2$](PF$_6$)$_2$ recorded in acetone-d6 at 233 K.

Even though the complex [Ni(pbss)Ru(bpy)$_2$]$^{2+}$ could adopt different conformations in solution, the conformation found in the X-ray structure is fully retained in solution. As the ruthenium(II) ion is kinetically inert, dissociation and conformational reorganisation – necessary for the ruthenium center and the propylene bridge to bind to opposite sides of the nickel coordination plane – are not expected and indeed not observed. Fluxional behaviour of the propylene bridge, giving rise to boat/chair conformations, or flipping of the ethylene side arms of the ligand should be possible in solution. However, this is not observed in the NMR spectra. This may be caused by the relatively strong interaction between the nickel(II) ion and the *ortho*-proton (H$_6$) of the pyridyl ring A (Ni···H, 2.858 Å, see Fig. 5.2) that is pertained in solution, as supported by the observed downfield resonance at 10.02 ppm at 293 K. The interaction of the ortho-proton of pyridyl ring A with the methylene protons of the C1 and C3 carbons as seen in the X-ray crystal structure, makes the four pyridyl rings and all the methylene protons unequal; these interactions were unequivocally identified by the cross peaks observed in NOESY experiments with different mixing times.

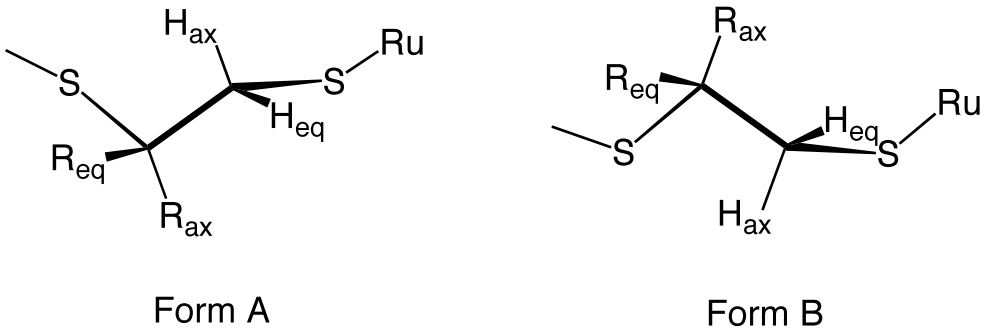

Fig. 5.5. Two observed conformations of [Ni(pbsms)Ru(bpy)$_2$](PF$_6$)$_2$ caused by the possible dynamic flipping of dimethylethylene arms.

The same type of interactions in solution are also exhibited by the complex [Ni(xbsms)Ru(bpy)$_2$](PF$_6$)$_2$ as e.g. shown by the resonance at 10.63 ppm, ascribed to the ortho H$_6$ proton of ring A, shifted downfield due to interaction with the nickel center, at

all the temperatures ranging between 233 and 303 K. Due to an interaction with the *ortho*-proton (H_6) of the pyridyl ring A, the methylene protons of the xylyl bridge are also shifted downfield to 4.97 ppm (Fig. 5.4). Thus also for [Ni(xbsms)Ru(bpy)$_2$]$^{2+}$ only one conformation of the compound is present in solution.

In contrast, for [Ni(pbsms)Ru(bpy)$_2$](PF$_6$)$_2$ eight sets of resonances are observed in the NMR spectra at low temperatures, which means that two different conformations of the complex are present in solution. In contrast to the two other complexes, interactions between the methylene protons of the C3 carbon in the propylene bridge and the ortho-protons of the pyridyl rings are not observed in both conformations of [Ni(pbsms)Ru(bpy)$_2$](PF$_6$)$_2$; this might suggest that the propylene bridge and the ruthenium center are now on opposite sides of the nickel coordination plane. An interaction between the pyridyl H_6 proton and a methylene proton of the dimethylethylene C1 carbon is observed in one of the two conformations, but not in the other, suggesting a dynamic flipping of the -CH_2–C(CH_3)$_2$– arms of the ligand pbsms. Based upon the observations it is concluded that the complex [Ni(pbsms)Ru(bpy)$_2$](PF$_6$)$_2$ shows one set of signals for form A, and another set of signals for form B as drawn in Fig. 5.5. This fluxional behaviour is not observed in the complex [Ni(xbsms)Ru(bpy)$_2$](PF$_6$)$_2$, possibly because the presence of the xylyl group prevents flipping of the dimethylethylene side arms; related complexes also show only one conformation in their ^{1}H NMR spectra.[2,3]

5.2.5. Electrochemical Behaviour of the [NiRu] Complexes

The cyclic voltammograms of the [NiRu] complexes were recorded in acetonitrile and dichloromethane solutions; relevant data are presented in Table 5.4. All three [NiRu] complexes exhibit a major reversible or quasi-reversible metal-based oxidation at around 1 V *vs*. Ag/AgCl in their cyclic voltammogram. This oxidation event is in the usual range for the Ru^{II}/Ru^{III} couple and these potentials are almost 400 mV more positive than the oxidation wave observed in the parent mononuclear nickel(II) complexes in dimethylformamide. The oxidation events are more reversible in dichloromethane solutions than in acetonitrile solutions for all three [NiRu] complexes. In contrast, the reduction waves are more reversible in acetonitrile. The complexes [Ni(pbsms)Ru(bpy)$_2$](PF$_6$)$_2$ and [Ni(xbsms)Ru(bpy)$_2$](PF$_6$)$_2$ show some minor redox couples around 0.6 V and 0.4 V *vs*. Ag/AgCl; these reductions are difficult to assign, due to the presence of multiple redox active partners. Also the [NiRu] complexes exhibit reduction waves around –0.90 V *vs*. Ag/AgCl, which are slightly less negative than in the parent mononuclear nickel(II) complexes in dimethylformamide. The complex [Ni(xbsms)Ru(bpy)$_2$](PF$_6$)$_2$ shows one more reduction wave at a more negative potential

(–1.39 V *vs*. Ag/AgCl) which may be caused by a reduction of the xylyl ligands; this reduction is not observed in the two other [NiRu] complexes.[37]

Table 5.4. Electrochemical data of the [NiRu] complexes in acetonitrile (dichloromethane). Measured using 0.5 mM solutions of complexes in acetonitrile containing 0.05 M $(NBu_4)PF_6$.*

Complex	E_{pa} (V)		E_{pc} (V)		ΔE (V)		E_{HER} (V)
$[Ni(pbss)Ru(bpy)_2](PF_6)_2$	1.02	(1.08)	0.79	(0.94)	0.166	(0.137)	–1.01
	–0.94	(–0.88)	–1.01	(–1.03)	0.073	(0.147)	
$[Ni(pbsms)Ru(bpy)_2](PF_6)_2$	0.93	(1.04)	0.80	(0.91)	0.132	(0.132)	–1.06
	0.64	(0.75)		(0.66)		(0.084)	
	0.38	(0.41)	0.32	(0.33)	0.056	(0.076)	
	–0.98	(–0.97)	–1.06	(–1.12)	0.080	(0.151)	
$[Ni(xbsms)Ru(bpy)_2](PF_6)_2$	0.91	(1.04)	0.79	(0.94)	0.115	(0.103)	–1.43
	0.70	(0.77)	0.62	(0.70)	0.081	(0.093)	
	0.36	(0.43)	0.31	(0.35)	0.048	(0.085)	
	–0.92		–1.01	(–0.99)	0.088		
	–1.39		–1.53		0.142		

* Scan rate 200 mV s^{-1}. Static GC disc working, Pt wire counter electrodes used with a Ag/AgCl (satd. KCl) reference electrode. The values in parenthesis are obtained using dichloromethane (0.5 mM) solutions of the [NiRu] complexes and are presented for comparison. E_{HER}: potential at which dihydrogen evolution reaction occurs.

The electrocatalytic proton reduction property of the $[Ni(S_2S'_2)Ru(bpy)_2](PF_6)_2$ complexes has been investigated using trifluoroacetic acid as the proton source. The addition of increasing amounts of trifluoroacetic acid to the solutions of the [NiRu] complexes results in an increase in the height of the reduction peaks in the case of $[Ni(pbss)Ru(bpy)_2](PF_6)_2$ (E_{HER} = –1.01 V *vs*. Ag/AgCl) and $[Ni(pbsms)Ru(bpy)_2](PF_6)_2$ (E_{HER} = –1.06 V *vs*. Ag/AgCl), whereas in the case of the complex $[Ni(xbsms)Ru(bpy)_2](PF_6)_2$ a new catalytic wave emerges and grows at –1.43 V *vs*. Ag/AgCl. The potential at which the proton reduction occurs is independent of the concentration of acid, unlike the [NiFe] complexes discussed in Chapter **3**, and only slightly moves to more negative potentials at higher concentrations of the acid. An interesting observation is that the oxidation potential of the complex $[Ni(pbss)Ru(bpy)_2](PF_6)_2$ shifts towards negative direction by 100 mV upon the addition of acid and thereafter remains stable at 0.91 V *vs*. Ag/AgCl. For the other two complexes the oxidation event stays unchanged even after the addition of increasing amounts of acid. Surprisingly, all three [NiRu] complexes are stable in the presence of 20 equivalents of trifluoroacetic acid for months as determined by ESI-MS spectrometry, showing the high acid tolerance of the complexes.

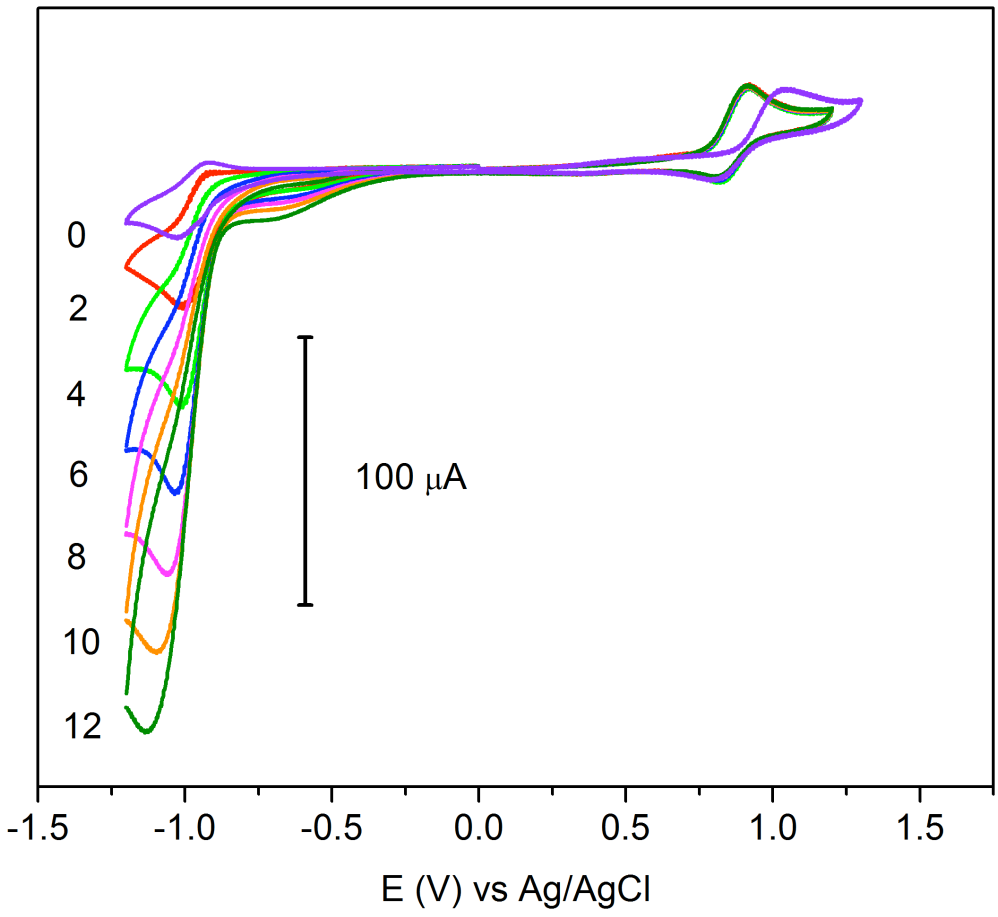

Fig. 5.6. Cyclic voltammograms of [Ni(pbss)Ru(bpy)$_2$](PF$_6$)$_2$ (0.5 mM) in acetonitrile in the presence of 0–12 equivalents of trifluoroacetic acid. Further details are provided in Table 5.4.

5.3. Discussion

The molecular structure of the complex [Ni(pbss)Ru(bpy)$_2$](PF$_6$)$_2$ is fully retained in solution, as indicated by ^{1}H NMR spectroscopy. The unsymmetrical nature of the molecular structure of the [Ni(pbss)Ru(bpy)$_2$](PF$_6$)$_2$, which leads to the four different sets of resonances for the four pyridyl rings in the ^{1}H NMR spectra, can be explained from the interaction between the nickel(II) ion and the *ortho*-proton of the one of the pyridyl rings as observed from the X-ray crystal structure data. The ortho proton H$_6$ of ring A (Fig. 5.2) is only 2.858 Å away from the nickel(II) ion in the crystal structure. This interaction is clearly reflected in the ^{1}H NMR spectra of the complex [Ni(pbss)Ru(bpy)$_2$](PF$_6$)$_2$ with the downfield shifted aromatic signal at 10.02 ppm (Table 5.3). The complexes [Ni(pbsms)Ru(bpy)$_2$](PF$_6$)$_2$ and [Ni(xbsms)Ru(bpy)$_2$](PF$_6$)$_2$ also exhibit the same interaction, as clearly indicated by resonances in the NMR spectra at 10.7 and 10.63 ppm, respectively.

The low-temperature ^{1}H NMR spectrum of complex [Ni(pbsms)Ru(bpy)$_2$](PF$_6$)$_2$ reveals the presence of two conformations in solution. Based on the available data it is proposed that these conformations are the A and B forms shown in Fig. 5.5; dynamic flipping of the dimethylethylene arms of the ligand is responsible for the two different forms. These two forms rapidly interconvert at room temperature, resulting in broad signals in the ^{1}H NMR spectra.

The NMR spectra of the complex [Ni(xbsms)Ru(bpy)$_2$](PF$_6$)$_2$ also show only one set of signals, indicating that in solution only one conformation is present. The related complex [Ni(xbsms)Ru(CO)$_2$Cl$_2$] has been structurally characterized; because of the steric repulsion of the methyl groups with the xylyl methylene groups of the Ni(xbsms) fragment, the ruthenium moiety is located on the same side of the nickel coordination plane as the aromatic ring of the [Ni(xbsms)] unit.[3] Flipping of the dimethylethylene arms is not observed and can be explained from this structure.[3]

Even though electron-donating dimethyl-substitution did not affect the reduction potentials to a large extent, the reduction potential of the complex [Ni(pbss)Ru(bpy)$_2$](PF$_6$)$_2$ (E_{pc}, –1.01 V *vs*. Ag/AgCl) is 0.05 V less negative than that of the complex [Ni(pbsms)Ru(bpy)$_2$](PF$_6$)$_2$ (E_{pc}, –1.06 V *vs*. Ag/AgCl) in acetonitrile. This difference also observed in the electrocatalytic reduction potential of these two complexes (Table 5.4). The electrocatalytic potential corresponding to the proton reduction is located at the same potential as the reduction of the complexes [Ni(pbss)Ru(bpy)$_2$](PF$_6$)$_2$ and [Ni(pbsms)Ru(bpy)$_2$](PF$_6$)$_2$, whereas for [Ni(xbsms)Ru(bpy)$_2$](PF$_6$)$_2$ the electrocatalytic wave appears 0.42 V more negative than the reduction potential of the complex. This difference may be indicative of different mechanisms followed by these complexes in the electrocatalytic proton reduction.

The protonation of the two thioether donors[38] leading to a metal-hydride intermediate can be excluded as these two thioether donors are most likely inert toward such protonation. However, the formation of metal-hydride species after protonation of the two thiolate bridging sulfur donors is more likely, as these bridging thiolates are known to bind with oxygen even in the form of Ni(μ–S$_2$)Ru. The reaction of benzene–1,2–dithiol with *cis*-[Ru(bpy)$_2$Cl$_2$] under argon followed by work-up in air produced the sulfinato complex [Ru(bpy)$_2$(C$_6$H$_4$S·SO$_2$)], which produced the complex [Ru(bpy)$_2$(C$_6$H$_4$SO$_2$·SO$_2$)] upon reaction with air.[37] However, extensive studies of combined spectroscopic methods are necessary to give further information concerning the electrocatalytic mechanism.

5.4. Conclusions

In summary, three novel [Ni($S_2S'_2$)Ru(bpy)$_2$](PF_6)$_2$ complexes have been synthesized and extensive structural characterisations have been made using NMR spectroscopy and X-ray crystallography. These complexes can be regarded as a new class of heterodinuclear [NiRu] compounds, which mimic the activity of the enzyme [NiFe] hydrogenase. All the three [NiRu] complexes have been shown to electrocatalyse the proton reduction and are highly stable in relatively high acid concentrations.

5.5. Experimental Procedures

5.5.1. General Remarks

The complexes [Ni(pbss)][31], [Ni(xbsms)][39] and *cis*-Ru(bpy)$_2$Cl$_2$·2H$_2$O[40] were synthesized according to the literature procedure. Synthesis and characterization of the mononuclear nickel complex [Ni(pbsms)] has been reported in Chapter **3**.

5.5.2. Synthesis of [Ni(pbss)Ru(bpy)$_2$](PF_6)$_2$

The *cis*-Ru(bpy)$_2$Cl$_2$·2H$_2$O (145 mg, 0.3 mmol) was refluxed in 10 ml ethanol for two hours to form [Ru(bpy)$_2$(EtOH)$_2$]Cl$_2$ in situ. Ni(pbss) (103 mg, 0.3 mmol) was added to this solution and the reaction mixture was refluxed overnight. NH_4PF_6 (97.8 mg, 0.6 mmol) was added to this reaction mixture when it was still hot and stirred for 10 minutes. The formed precipitate was filtered off and dried under vacuum to get the purple coloured powder of [Ni(pbss)Ru(bpy)$_2$](PF_6)$_2$ (222 mg, 75%). Purple coloured needles suitable for X-ray diffraction were obtained in one day by diffusing ether into acetone solution of the complex. **Elemental analysis (%):** calculated for $C_{27}H_{30}N_4NiRuS_4F_{12}P_2$·0.7$CH_2Cl_2$: C 31.75, H 3.02, N 5.35, S 12.24; found: C 31.75, H 2.92, N 5.32, S 12.11. **MS (ESI):** (*m/z*) calculated for $NiRuC_{27}H_{30}N_4S_4$ [M–(PF_6)$_2$]$^{2+}$ requires (monoisotopic mass) 348.99, found 348.80 (with expected isotopic distribution).

5.5.3. Synthesis of [Ni(pbsms)Ru(bpy)$_2$](PF_6)$_2$

This complex was synthesized by following the same procedure as in section 5.5.2. **Yield:** 69%. **Elemental analysis (%):** calculated for $C_{31}H_{38}N_4NiRuS_4F_{12}P_2$: C 35.64, H 3.67, N 5.36, S 12.28; found: C 35.87, H 3.58, N 5.48, S 12.07. **MS (ESI):** (*m/z*) calculated for $NiRuC_{27}H_{30}N_4S_4$ [M-(PF_6)$_2$]$^{2+}$ requires (monoisotopic mass) 377.02, found 376.86 (with expected isotopic distribution).

5.5.4. Synthesis of [Ni(xbsms)Ru(bpy)$_2$](PF_6)$_2$

This complex was synthesized by following the same procedure as in section 5.5.2. **Yield:** 81%. **Elemental analysis (%):** calculated for $C_{36}H_{40}N_4NiRuS_4F_{12}P_2$: C 39.07, H 3.64,

N 5.06, S 11.59; found: C 39.09, H 3.66, N 5.11, S 11.38. **MS (ESI):** (*m/z*) calculated for $NiRuC_{27}H_{30}N_4S_4$ $[M-(PF_6)_2]^{2+}$ requires (monoisotopic mass) 408.03, found 407.72 (with expected isotopic distribution).

5.5.5. X-ray crystal structure determinations

Crystallographic data for $[Ni(pbss)Ru(bpy)_2][PF_6]_2$. $C_{27}H_{30}N_4NiRuS_4F_{12}P_2$, Fw = 988.51, dark brown needles, 0.10 × 0.22 × 0.24 mm^3, monoclinic, $P2_1/c$ (no. 14), a = 17.8350(2), b = 9.0801(1), c = 26.2556(6) Å, β = 112.470(2), V = 3929.12(12) $Å^3$, Z = 4, D_x = 1.671 g cm^{-3}, μ = 1.240 mm^{-1}. 59429 Reflections were measured up to a resolution of $(\sin\theta/\lambda)_{max}$ = 0.65 $Å^{-1}$. An absorption correction based on multiple measured reflections was applied (0.33–0.0.86 correction range). 9004 Reflections were unique (R_{int} = 0.038), of which 7225 were observed [I > 2σ(I)]. 460 Parameters were refined with no restraints. $R1/wR_2$ [I > 2σ(I)]: 0.0203/0.0387. $R1/wR_2$ [all refl.]: 0.0303/0.0619. S = 1.05. Residual electron density between −0.62 and 0.57 $eÅ^{-3}$. The program SQUEEZE (PLATON) was used to eliminate the electronic contribution of ill-defined solvent.

5.6. References

1. S. Canaguier, V. Artero and M. Fontecave, *Dalton Trans.*, 2008, 315-325.
2. Y. Oudart, V. Artero, J. Pecaut, C. Lebrun and M. Fontecave, *Eur. J. Inorg. Chem.*, 2007, 2613-2626.
3. Y. Oudart, V. Artero, J. Pecaut and M. Fontecave, *Inorg. Chem.*, 2006, **45**, 4334-4336.
4. M. A. Reynolds, T. B. Rauchfuss and S. R. Wilson, *Organometallics*, 2003, **22**, 1619-1625.
5. B. Kure, T. Matsumoto, K. Ichikawa, S. Fukuzumi, Y. Higuchi, T. Yagi and S. Ogo, *Dalton Trans.*, 2008, 4747-4755.
6. S. Ogo, R. Kabe, K. Uehara, B. Kure, T. Nishimura, S. C. Menon, R. Harada, S. Fukuzumi, Y. Higuchi, T. Ohhara, T. Tamada and R. Kuroki, *Science*, 2007, **316**, 585-587.
7. A. K. Justice, R. C. Linck and T. B. Rauchfuss, *Inorg. Chem.*, 2006, **45**, 2406-2412.
8. A. K. Justice, R. C. Linck, T. B. Rauchfuss and S. R. Wilson, *J. Am. Chem. Soc*, 2004, **126**, 13214-13215.
9. A. Volbeda, E. Garcia, C. Piras, A. L. deLacey, V. M. Fernandez, E. C. Hatchikian, M. Frey and J. C. FontecillaCamps, *J. Am. Chem. Soc.*, 1996, **118**, 12989-12996.
10. A. Volbeda, M. H. Charon, C. Piras, E. C. Hatchikian, M. Frey and J. C. Fontecilla-Camps, *Nature*, 1995, **373**, 580-587.
11. H. Ogata, S. Hirota, A. Nakahara, H. Komori, N. Shibata, T. Kato, K. Kano and Y. Higuchi, *Structure*, 2005, **13**, 1635-1642.
12. H. Ogata, Y. Mizoguchi, N. Mizuno, K. Miki, S. Adachi, N. Yasuoka, T. Yagi, O. Yamauchi, S. Hirota and Y. Higuchi, *J. Am. Chem. Soc.*, 2002, **124**, 11628-11635.
13. Y. Higuchi, H. Ogata, K. Miki, N. Yasuoka and T. Yagi, *Structure*, 1999, **7**, 549-556.
14. Y. Higuchi, T. Yagi and N. Yasuoka, *Structure*, 1997, **5**, 1671-1680.
15. A. Volbeda, L. Martin, C. Cavazza, M. Matho, B. W. Faber, W. Roseboom, S. P. J. Albracht, E. Garcin, M. Rousset and J. C. Fontecilla-Camps, *J. Biol. Inorg. Chem.*, 2005, **10**, 239-249.
16. A. Volbeda, Y. Montet, X. Vernede, E. C. Hatchikian and J. C. Fontecilla-Camps, *Int. J. Hydrog. Energy*, 2002, **27**, 1449-1461.
17. Y. Montet, P. Amara, A. Volbeda, X. Vernede, E. C. Hatchikian, M. J. Field, M. Frey and J. C. FontecillaCamps, *Nat. Struct. Biol.*, 1997, **4**, 523-526.
18. P. M. Matias, C. M. Soares, L. M. Saraiva, R. Coelho, J. Morais, J. Le Gall and M. A. Carrondo, *J. Biol. Inorg. Chem.*, 2001, **6**, 63-81.

19. E. Garcin, X. Vernede, E. C. Hatchikian, A. Volbeda, M. Frey and J. C. Fontecilla-Camps, *Structure*, 1999, **7**, 557-566.
20. J. K. Law, H. Mellows and D. M. Heinekey, *J. Am. Chem. Soc.*, 2002, **124**, 1024-1030.
21. S. Ott, M. Borgstrom, M. Kritikos, R. Lomoth, J. Bergquist, B. Åkermark, L. Hammarström and L. C. Sun, *Inorg. Chem.*, 2004, **43**, 4683-4692.
22. S. Ott, M. Kritikos, B. Akermark and L. C. Sun, *Angew. Chem.-Int. Edit.*, 2003, **42**, 3285-3288.
23. H. Wolpher, M. Borgstrom, L. Hammarstrom, J. Bergquist, V. Sundstrom, S. Stenbjorn, L. C. Sun and B. Akermark, *Inorg. Chem. Commun.*, 2003, **6**, 989-991.
24. J. Ekström, M. Abrahamsson, C. Olson, J. Bergquist, F. B. Kaynak, L. Eriksson, S. C. Licheng, H. C. Becker, B. Åkermark, L. Hammarström and S. Ott, *Dalton Trans.*, 2006, 4599-4606.
25. A. M. Kluwer, R. Kapre, F. Hartl, M. Lutz, A. L. Spek, A. M. Brouwer, P. W. N. M. van Leeuwen and J. N. H. Reek, *Proc. Natl. Acad. Sci. U. S. A.*, 2009.
26. L. C. Song, M. Y. Tang, S. Z. Mei, J. H. Huang and Q. M. Hu, *Organometallics*, 2007, **26**, 1575-1577.
27. X. Q. Li, M. Wang, S. P. Zhang, J. X. Pan, Y. Na, J. H. Liu, B. Akermark and L. C. Sun, *J. Phys. Chem. B*, 2008, **112**, 8198-8202.
28. A. Fihri, V. Artero, A. Pereira and M. Fontecave, *Dalton Trans.*, 2008, 5567-5569.
29. A. Fihri, V. Artero, M. Razavet, C. Baffert, W. Leibl and M. Fontecave, *Angew. Chem.-Int. Edit.*, 2008, **47**, 564-567.
30. Y. Na, M. Wang, J. X. Pan, P. Zhang, B. Åkermark and L. C. Sun, *Inorg. Chem.*, 2008, **47**, 2805-2810.
31. T. Yamamura, H. Arai, N. Nakamura and H. Miyamae, *Chem. Lett.*, 1990, 2121-2124.
32. M. A. Halcrow and G. Christou, *Chem. Rev.*, 1994, **94**, 2421-2481.
33. D. Sellmann, D. Haussinger and F. W. Heinemann, *Eur. J. Inorg. Chem.*, 1999, 1715-1725.
34. W. F. Zhu, A. C. Marr, Q. Wang, F. Neese, D. J. E. Spencer, A. J. Blake, P. A. Cooke, C. Wilson and M. Schröder, *Proc. Natl. Acad. Sci. U. S. A.*, 2005, **102**, 18280-18285.
35. T. Yoshimura, A. Shinohara, M. Hirotsu, K. Ueno and T. Konno, *Bull. Chem. Soc. Jpn.*, 2006, **79**, 1745-1747.
36. T. Yoshimura, A. Shinohara, M. Hirotsu and T. Konno, *Chem. Lett.*, 2005, **34**, 1310-1311.
37. R. A. Begum, A. A. Farah, H. N. Hunter and A. B. P. Lever, *Inorg. Chem.*, 2009, **48**, 2018-2027.
38. R. Angamuthu and E. Bouwman, *Phys. Chem. Chem. Phys.*, 2009, **11**, 5578–5583.
39. J. A. W. Verhagen, D. D. Ellis, M. Lutz, A. L. Spek and E. Bouwman, *J. Chem. Soc.-Dalton Trans.*, 2002, 1275-1280.
40. B. P. Sullivan, D. J. Salmon and T. J. Meyer, *Inorg. Chem.*, 1978, **17**, 3334-3341.